Automatic Location of Ventricular Arrhythmia using Implantable Defibrillator Stored Electrograms

M Sanroman-Junquera[1], I Mora-Jimenez[1], J Almendral[2,3], E Everss[1], A Caamaño-Fernandez[1], F Atienza[4], L Castilla[4], JL Rojo-Alvarez[1]

[1]Signal Theory and Communications Department, Rey Juan Carlos University, Spain
[2]Cardiology Department, Hospital General Universitario Gregorio Marañon, Madrid, Spain
[3]Electrophysiology Unit. Grupo Hospital de Madrid, Universidad CEU-San Pablo, Madrid, Spain

Abstract

Electrograms (EGM) stored in Implantable Cardioverter Defibrillator (ICD) during ventricular tachycardia episodes have recently been shown to convey valuable information for the identification of the anatomical origin of the arrhythmia and subsequent ablation therapy. We developed an automatic procedure for estimating the focal origin of the arrhythmia by analyzing the EGM waveforms. A clinical protocol was designed for validation, consisting of electrical pacing from different spatial locations in the left ventricle, in which the spatial coordinates of the pacing electrode were known by the use of a sequential navigation system. EGM from can-coil lead configuration were stored in the ICD for 25 patients (18 ± 10.1 *EGM per patient). Several machine learning classifiers (k nearest neighbors, radial basis function, and multilayer perceptron), were implemented, whose input space was given by the 201 samples (340 ms) of the template for each pacing location, and by a set of simple parameters selected according to clinical criteria. The target output was set by considering the heart division in three main planes, hence giving jointly 8 possible classification regions (octants). To estimate the generalization performance, classification was evaluated following a leave-one-patient-out strategy. Location accuracy reached 73%, 58.4%, 57.5% (for binary classification in terms of main planes), and for octant identification with multioutput classification reached 36.3% (note that the random 8-output classifier average accuracy rate is 12.5%). We can conclude that the estimation of the arrhythmia location can be addressed by analyzing the EGM waveform and features using learning from samples techniques.*

1. Introduction

Implantable Cardioverter Defibrillator (ICD) is a usual prevention for patients with previous Ventricular Tachycardia (VT), being an effective therapy in preventing sudden cardiac death episodes [1]. This device detects automatically a dangerously fast heart rhythm and, when necessary, it delivers appropriate therapy (pacing, low-energy cardioversion or high-energy shocks) in order to restore the sinus rhythm. A number of ventricular arrhythmias are due to ectopic focuses or accessory pathways, and they can be suppressed by means of cardiac ablation in electrophysiological studies, in which radiofrequency energy or intense cold is used to sear the abnormal tissue with a catheter inserted into the heart chamber [2].

The correct location of arrhythmogenic sources is crucial to ensure the success of ablation therapy. Among other devices, the Sequential Navigation Systems (SNS) are often used by electrophysiologists to guide the catheter ablation procedure [3]. Current SNSs yield the catheter spatial location at each moment, and sequentially build a three-dimensional reconstruction of the heart chamber geometry. This represents useful complementary information to the catheter-sensed intracardiac electrograms (EGM), and they are jointly considered to build feature maps, such as activation or voltage. Some studies have shown that the morphology of arrhythmic electrical recordings provides relevant information about the arrhythmia origin [4], and hence, it would be helpful for the electrophysiologist a system capable of automatically providing the heart region for ablation target, based on previously observed EGM arrhythmic recordings.

In this setting, the main problem is the availability of recordings for the validation of the spatial origin in spontaneous arrhythmias. In this work, we use: (1) the monomorphic arrhythmia intracardiac recordings from pacing during electrophysiological study as representative of the ICD stored EGM waveforms during VT; and (2) the simultaneously recorded coordinates of the pacing electrode in a SNS, which gives the spatial location information. This data configuration allows us to design an statistical classifier, based on the arrhythmia morphology and on simple

parameters, with automatically indicates the origin for left ventricle originated arrhtyhmias.

The scheme of the paper is as follows. In the next section, the clinical database is described. Then, the statistical classification procedures used for estimating the anatomical origin of the arrhythmia are summarized. Results in the clinical database show the performance that can be obtained with several classification configurations.

2. Clinical database

All the EGM during pacing and their corresponding spatial locations came from electrophysiological studies at the Hospital General Universitario Gregorio Marañón in Madrid (Spain). The EGMs, obtained during cardiac stimulation (pacing) in different parts of the left ventricle (LV), were stored in ICD (Medtronic®), and the pacing coordinates were obtained using the Carto™XP navigation system. The EGMs were available from two different lead configuratins (from subpectoral can to the coil in the right ventricle, and from tip to ring both in the right ventricle), and they were directly retrieved from the ICD using telemetry, and they were printed on paper, hence allowing to recover the recording in digital format after digital image processing techniques [5]. Recordings (460 altogether) were collected between December 2003 and November 2008, in 25 patients (2 women and 23 men), 18.4 ± 1.10 (M $\pm$ STD) EGM per patient. Patients with cardiac arrhythmias and with ICD were considered. Pacing protocol at each LV site was made using a train of at least 10 beats of fast ventricular stimulation with cycle 400 or 500 ms. The intensity of the applied current was initially 5 mA, and it increased if necessary to ensure capture.

The spatial location of the arrhythmia was obtained with the three-dimensional nonfluoroscopic mapping system, which allowed us to obtain a LV endocardial map. By using the tool software *design a line*, an expert electrophysiologist drew several lines on the map, hence dividing the LV in two halves: septal vs lateral (Halves-1), superior vs inferior (Halves-2), and apical vs basal (Halves-3), as shown in Figure 1. The intersection of these three lines generated a division into eight regions. Each of these regions was called an octant, and they were defined as superior-septal-apical (SSA), septal-superior-basal (SSB), septal-inferior-apical (SIA), septal-inferior-basal (SIB) , lateral-superior-apical (LSA), lateral-superior-basal (LSB), lateral-inferior-apical (LIA), and basal-lateral-inferior (LIB).

3. Statistical learning procedure

From an statistical learning perspective, the aforementioned partition of the LV into eight regions allows us to locate the focal origin of the arrythmia with two kinds of

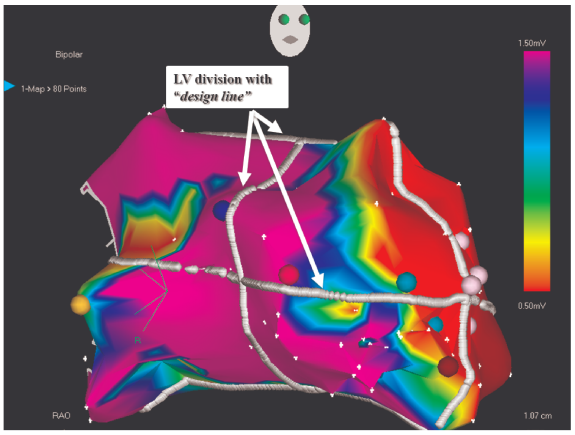

Figure 1. Example of voltage map in the LV from Carto^{TM}XP system.

classifiers. On the one hand, a multiclass classifier can be used in order to determine the location from one of the eight regions. On the other hand, it is also possible to simplify the classifier design and construct the final classifier as the combination of three binary classifiers, each considering the location on one of two LV halves (Halves-1, Halves-2, and Halves-3).

3.1. Input spaces

From the recordings of the can-coil lead configuration, we built two datasets: C1, which characterized the beat waveform in the time domain; and C2, which used some representative parameters extracted from the corresponding beat waveform.

Dataset C1 had 201 attributes, each corresponding to the voltage of the representative beat waveform in a different time instant. For every patient, one representative beat waveform (template from now on) was obtained in every pacing site by averaging the available beats (see Figure2).

From a machine learning point of view, the use of high dimensional data can make difficult the classifier design [6]. The curse of dimensionality states that, as the number of attributes increases, it becomes exponentially more difficult to find a fitting model (in this case, a classifier). To alleviate this problem, we obtained semi-automatically from every template three parameters (with clinical interpretation) as indicated in Figure 2, hence constructing the dataset C2 described as next:

- t_{so}: time interval between the stimulus and the onset of can-coil template.
- v_{IP}: voltage ratio between initial deflection and peak deflection, the last one being the largest voltage above the baseline. Initial deflection is the smallest voltage (almost always negative) between the onset of can-coil EGM and the peak deflection.

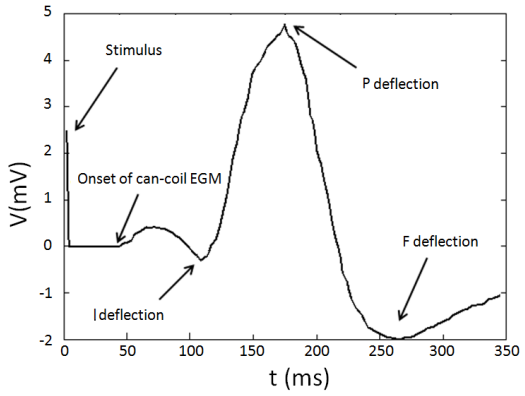

Figure 2. Waveform of a representative template and fiducial points used to extract the amplitude and time parameters in a can-coil ICD stored EGM.

• v_{FP}: voltage ratio between the final deflection and peak deflection. Final deflection is the smallest voltage between the peak deflection and the end of the template.

The classifier design was tackled by considering independently both datasets (C1 and C2).

3.2. Statistical classifiers

We considered three classification schemes: voting k-Nearest Neighbors (k-NN), which represents an instance-based classifier approaching the Bayes error rate with increasing amount of data [7]; and two neural networks (NN), which represent universal function aproximators, namely, the Radial Basis Function Network (RBFN), and the Multi-Layer Perceptron (MLP) [6].

The voting k-NN classifier relies on an estimation of the *a posteriori* probability, assigning a datum to the most representative class among that of the k nearest data in the training dataset. As the distance metric, the standard Euclidean distance was used.

We considered for both NNs the simplest architecture with three layers (input, hidden, and output). Regarding the hidden neurons, we used spherical Gaussian radial basis functions for the RBFN, and standard sigmoidal neurons for the MLP. In the multiclass classifier, the output layer consisted of three neurons (one for each half, hence providing eight different regions); for the binary classifier, the output layer had just one neuron.

For training the RBFN, we considered a fast sequential learning approach. First, the centers and widths of the hidden neurons were set with the Expectation-Maximization algorithm. Then, the weights connecting the hidden and the output neurons were determined by applying the Moore-Penrose pseudo-inverse. The MLP network was trained using the conjugate gradient algorithm to minimize the sum-of-squared errors and thus find, simultaneously, the hidden and output weights.

When working with statistical classifiers, it is convenient to preprocess the data for all the input attributes being in a similar range (normalization), hence avoiding an input attribute dominating and hiding others due to a scaling effect [6]. Among all the available normalization procedures, we used the zero mean and unit standard deviation normalization (m=0,σ=1) and the bounded interval normalization to [-1,1].

To get an accurate estimation of the generalization performance, we used the following procedure, called *leave one patient out* for its similarity with the leave-one-out scheme [7]: (1) set apart all the templates of one patient; (2) train the classifier with the templates of the remainder patients; and (3) evaluate the performance of the trained classifier with the templates of the patient not used for training. This procedure was repeated 25 times (one for every patient in the database), and the generalization performance was computed as the average performance of the 460 templates not used during training.

To design the classifiers, we explored a range of values for each design parameter:

• For parameter k in the k-NN approach, values between $k = 1$ and $k = 50$ (step of 1) were considered.

• For the number of hidden neurons in the NN approaches, the range from 1 to 10 was evaluated.

For each classifier, the most appropriate value was chosen according to a 5-fold cross validation methodology [7].

4. Results

Results in Table 1 show the accuracy of the three classifiers averaged over 10 runs using the *leave one patient out* method. Both binary and multiclass classifiers have been benchmarked. Results in multiclass column of octants group were obtained for a single multiclass classifier structure, whereas binary column shows the results for three binary classifiers combined for a multiclass strategy. Design parameters (k for kNN and number of hidden units for NNs) from 5-fold cross validation are also presented, in braces (mean, standard deviation) below the accuracy figures. Training process was made both for normalized and not normalized input attributes. The table shows the best obtained results, corresponding to not normalizing. We found that (m=0,σ=1)-normalization did not improve and [-1,1]-normalization degraded significantly the performance.

Similar performance was in general obtained for octants-based classifiers when the same classifier is considered, with an slightly lower classification rate for the C1 dataset (named waveform in the table), probably due to the high number of input attributes. Recall that the random

Table 1. Averaged (and standard deviation) percentage of accuracy, for the classifiers in sets C1 and C2.

		Octants		Halves		
Classifier	**Atributes**	Binary combination	Multiclass	Halves-1	Halves-2	Halves-3
k-NN	Waveform	33.7(0.2)	19.4(0.1) {1.3(0.1)}	70.5(0.1) {13.2(0.1)}	58.4(0.1) {1.4(0.0)}	55.0(0.1) {3.4(0.0)}
	t_{so},v_{IP},v_{FP}	22.8(0.2)	22.5(0.2) {36.9(0.4)}	72.8(0.0) {37.8(0.3)}	58.2(0.1) {33.6(0.3)}	55.9(0.2) {36.9(0.3)}
	v_{IP},v_{FP}	24.7(0.2)	22.6(0.3) {31.6(1.0)}	72.8(0.0) {23.5(0.1)}	58.5(0.0) {10.7(0.3)}	57.1(0.2) {37.1(0.3)}
RBF	t_{so},v_{IP},v_{FP}	30.9(4.0)	35.5(1.6) {3.8(0.9)}	71.9(0.6) {3.4(0.7)}	58.1(1.8) {3.1(0.7)}	57.2(1.1) {2.9(0.5)}
	v_{IP},v_{FP}	35.3(1.4)	33.0(1.2) {2.3(0.8)}	71.7(0.8) {1.0(0.0)}	54.1(1.3) {1.0(0.0)}	52.8(1.2) {1.0(0.0)}
MLP	Waveform	31.0(1.2)	33.8(1.9) {1.1(0.4)}	69.5(1.3) {1.2(0.5)}	56.3(1.4) {1.1(0.4)}	49.7(1.5) {1.1(0.3)}
	t_{so},v_{IP},v_{FP}	35.9(1.6)	34.8(1.3) {3.2(1.0)}	73.1(0.3) {1.2(0.5)}	57.4(2.4) {2.4(1.4)}	57.1(1.1) {1.4(1.0)}
	v_{IP},v_{FP}	36.3(1.2)	36.2(1.1) {2.5(0.8)}	73.1(1.0) {1.4(0.7)}	56.0(1.6) {1.9(1.1)}	57.5(1.8) {1.7(1.2)}

8-output classifier average accuracy rate is 12.5%. Reduction in the difficulty of the classifier design, going from classification into 8 regions (octants column) to that into 2 halves (binary combination column), usually led to an improvement in the classification rate, especially remarkable for the k-NN classifier. NNs classifiers with parameter-based input spaces reached in general higher performance than waveform-based k-NN. Waveform-based MLP classifier had a performance slightly lower than k-NN (except for multiclass classifier), and waveform-based RBF was not calculated due to numeric issues in the Moore-Penrose calculation.

Halves, binary classifiers yielded similar results for different input spaces, and for different classifiers. Actually, binary strategy gave slightly better classification than a random classifier for Halves-2 and Halves-3, whereas performance was markedly higher for Halves-1.

With respect to the machine complexity in the parameter-based input space NNs classifiers, it was comparable to the input space dimensionality, hence the classification can be done with controlled complexity systems. Slightly higher complexity was necessary for octants-based classifiers. Only limited complexity (up to 10 neurons) was explored in the waveform-based MLP schemes, due to computational issues and for avoiding the curse of the dimensionality.

5. Conclusions

The automatic location of the anatomical origin of ventricular tachycardias can be estimated by analyzing ICD stored EGM morphology and simple features. Statistical learning algorithms with limited complexity can be used for this purpose. The validation protocol included merging data from SNS and EGM in ICD during pacing at electrophysiological studies, giving an adequate gold standard for this application.

References

[1] Hernandez A, Fonarow G, Hammill B, et al. Clinical effectiveness of implantable cardioverter-defibrillators among medicare beneficiaries with heart failure. Circulation 2010; 3:7–13.

[2] Scheinman M, Huang S. The 1998 naspe prospective catheter ablation registry. Pacing and Clinical Electrophysiology 2000;23:1020–1028.

[3] Pruszkowska-Skrzep P, Kalarus Z, Sredniawa B, et al. Effectiveness of radiofrequency catheter ablation of right ventricular outflow tract tachycardia using the carto system. Kardiol Pol 2005;62:138–144.

[4] Almendral J, Atienza F, et al. Implantable defibrillator electrograms and origin of left ventricular impulses: an analysis of regionalization ability and spatial resolution. Under review 2010;.

[5] Sanromán-Junquera M, Mora-Jiménez I, Everss E, Almendral-Garrote J, García-Alberola A, Atienza F, Castilla-SanJosé L, Rojo-Álvarez J. Quality evaluation and effect of time syncronization on the digital recovery of intracardiac electrograms. In Computers in Cardiology 2009. Park City, Utah, 2009; 801–804.

[6] Haykin S. Neural networks and learning machines. Pearson International Edition, 2009.

[7] Duda R, Hart P, Stork D. Pattern Classification. Wiley-Interscience, John Wiley and Sons, Inc., 2001.

Address for correspondence:

Margarita Sanromán-Junquera
B-013, Universidad Rey Juan Carlos
Camino del Molino s/n, 28947-Fuenlabrada, Madrid (Spain)
E-mail to m.sanromanj@alumnos.urjc.es